Supporting information

Directed Self-Assembly of Colloidal Particles onto Nematic Liquid Crystalline Defects Engineered by Chemically Patterned Surfaces

Xiao Li,[1,2 &] Julio C. Armas-Pérez,[1,3 &] Juan P. Hernández-Ortiz,[4,1] Christopher G. Arges,[1, 5] Xiaoying Liu,[1] José A. Martínez-González,[1] Leonidas E. Ocola,[2] Camille Bishop,[1] Helou Xie,[1] Juan J. de Pablo[1,2*] and Paul F. Nealey[1,2*]

[1] Institute for Molecular Engineering, University of Chicago, Chicago, Illinois 60637
[2] Argonne National Laboratory, 9700 South Cass Avenue, Argonne, IL 60439, USA
[3] División de Ciencias e Ingenierías, Campus León, Universidad de Guanajuato, Loma del Bosque 103, León (Gto.) 37150, Mexico
[4] Departamento Materiales y Minerales, Universidad Nacional de Colombia -- Medellin, Calle 75 # 79A-51, Bloque M17, Medellin, Colombia
[5] Cain Department of Chemical Engineering, Louisiana State University, Baton Rouge, Louisiana 70803, USA

[*] Corresponding authors: nealey@uchicago.edu and depablo@uchicago.edu

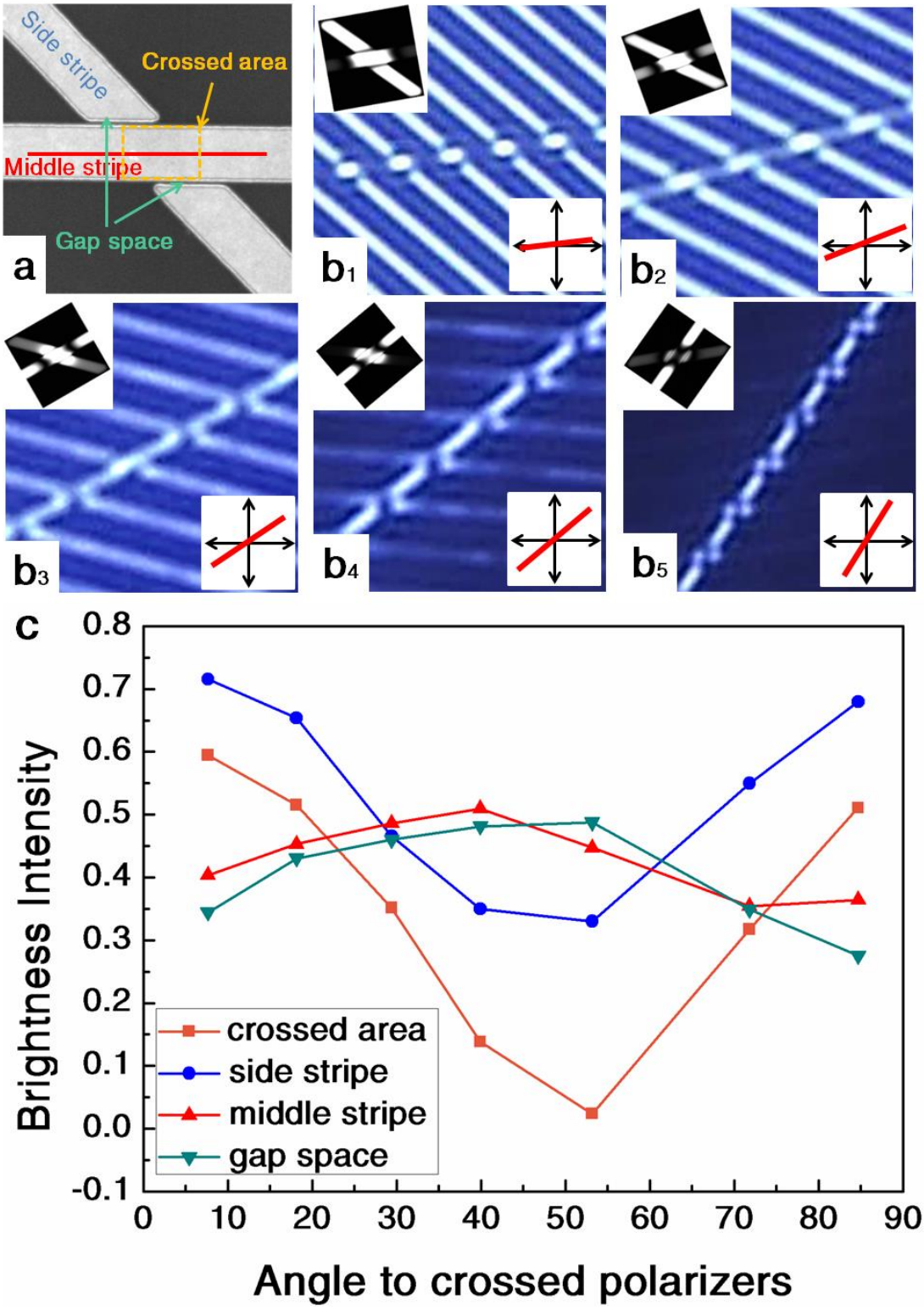

Figure S1 | Reflective light microscope images of the 5CB cell under crossed polarizers by different rotation angle. (a) SEM image of disjoint stripe pattern with S_w = Mw = 500 nm, G_w = 50nm, the middle stripe, side stripe, crossed point and gap space were marked. (b_1-b_5) The reflective light microscopy images of the 5CB cell under the crossed polarizers at different rotation angles relative to the crossed polarizer, which were marked in the inner images. (c) The brightness intensity of the

middle stripe, side stripe, crossed point and gap space was calculated as function of different rotation angles.

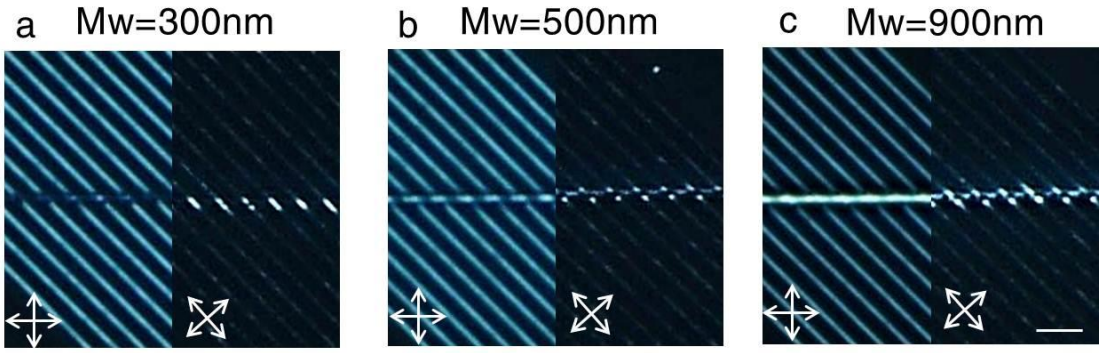

Figure S2 | The reflective light microscopy images of the cell under crossed polarizers. The 5CB cell (*H* = 1.5 μm) with different middle stripe width of the disjoint stripe patterns on the PMMAZO brush substrate: (a) *Mw* = 300 nm; (b) *Mw* = 500 nm; (c) *Mw* = 900 nm.

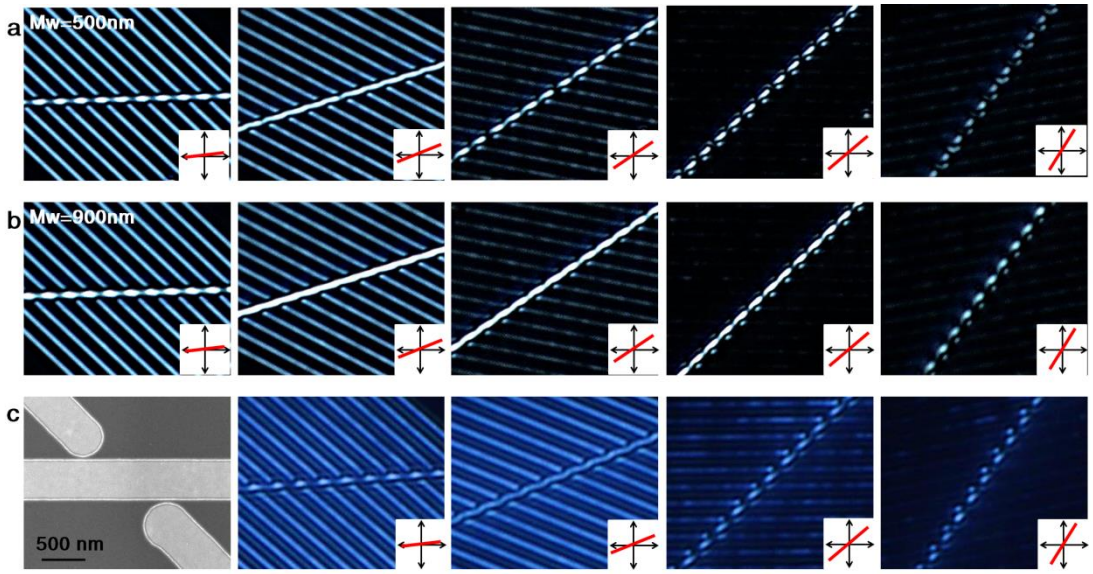

Figure S3 | The reflective light microscopy images of 5CB mixture with colloids under the crossed polarizers. The 45° angle of disjoint stripe patterns with different middle stripe width (a) M_w = 500 nm; (b) M_w = 900 nm were showed at different rotation angles relative to the crossed polarizer, which were marked in each of inner images. (c) SEM image of disjoint stripe pattern with side stripe ended as round shape, $S_w = M_w$ = 500 nm and G_w = 50 nm; Polarizing microscopy image of nematic 5CB cell with the bottom surface of the round end disjoint stripe pattern. The direction of middle stripe to the crossed polarizes was marked.

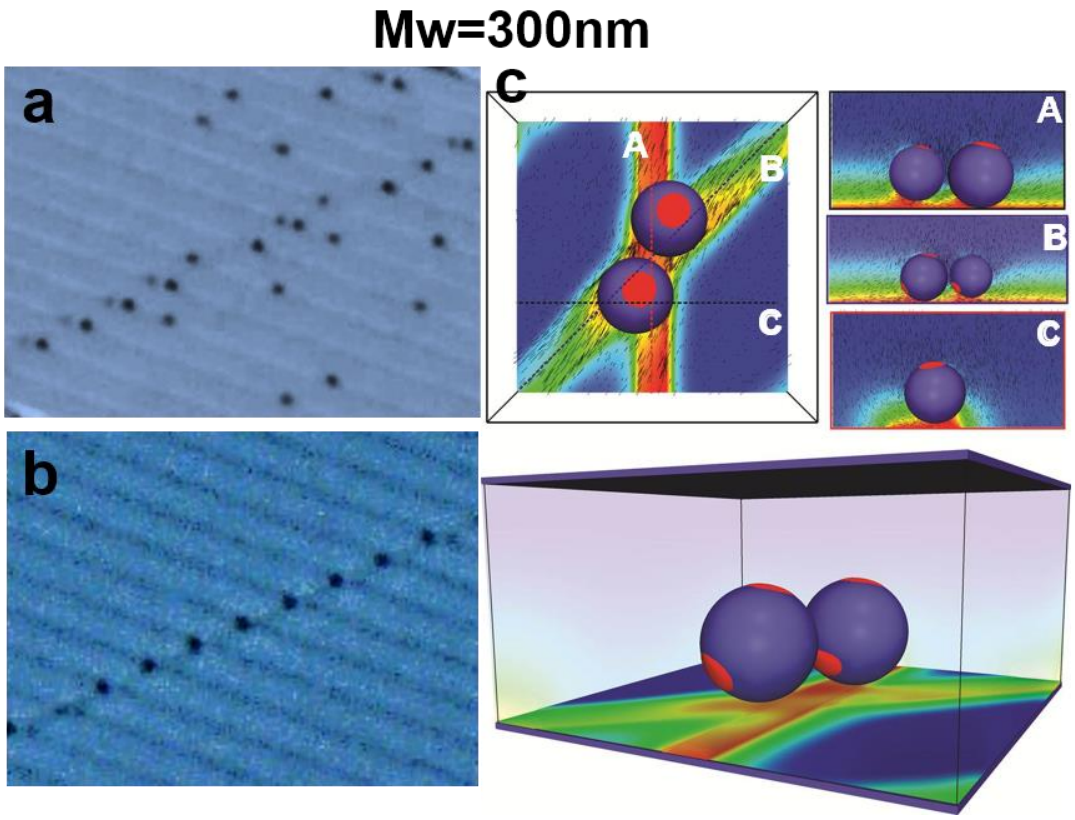

Figure S4 | Trapped colloidal particles at the gap spaces on patterned substrates. The reflective light microscopy images of the trapped PS colloidal particles in 5CB cell (H = 1.5 μm) under the paralleled polarizers with middle stripe width M_w = 300 nm: (a) colloidal particle diameter = 800 nm; (b) colloidal particle diameter = 1 μm. (c) Schematic representation of the polystyrene colloidal particles trapped at the gap spaces obtained by simulation in the Landau-de Gennes framework, showing the director fields effected by the two colloidal particles and defects regions generated on two colloids.

THERMODYNAMIC DESCRIPTION

The thermodynamic state of the LC is described in terms of the local alignment tensor $\boldsymbol{Q}(\boldsymbol{x})$, defined in terms of the second moment of the local molecular orientational distribution function, $\psi(u, x, t)$:

$$\mathbf{Q}(\mathbf{x}) = \int (\mathbf{uu} - \frac{\boldsymbol{\delta}}{3})\psi(\mathbf{u}, \mathbf{x}, t)d\mathbf{u}, \quad (1)$$

where $\boldsymbol{u}(\boldsymbol{x})$ is the ensemble average of molecular orientations and $\boldsymbol{\delta}$ is the 3 × 3 identity matrix. The tensor order parameter in Eqn. (1) includes all relevant information regarding the ensemble average alignment of LC molecules, *i.e.* directions and level of order, as indicated by its eigenvalues and eigenvectors. Therefore, the alignment tensor $\boldsymbol{Q}(\mathbf{x})$ may be written as [1, 2]

$$\mathbf{Q} = S\left[\mathbf{nn} - \frac{\delta}{3}\right] + \eta\left[\mathbf{n}'\mathbf{n}' - (\mathbf{n} \times \mathbf{n}')(\mathbf{n} \times \mathbf{n}')\right], \quad (2)$$

where $S(\boldsymbol{x})$ is the scalar order parameter, related to the maximum eigenvalue $2S/3$, and $\eta(\boldsymbol{x})$ is the biaxiality, related to the other two eigenvalues $\pm\eta - S/3$. The eigenvectors, n and n′, corresponding to the maximum and second largest eigenvalues, respectively, define an orthonormal basis $\{n, n', (n \times n')\}$ for LC orientation. The scalar order parameters, S and η, are bounded by:

$$S \in [-\frac{1}{2}, 1] \quad \text{and} \quad \eta \in [-\frac{1}{3}(1 - S), +\frac{1}{3}(1 - S)] \quad (3)$$

The free energy functional consists of the sum of three terms: a short-range Landau polynomial expansion of the tensor invariants to describe the isotropic-nematic (IN) transition, a long-range free energy density that penalizes elastic distortions, and a surface free energy contribution, given by

$$F(\mathbf{Q}, \nabla\mathbf{Q}, E_f) = \int d^3\mathbf{x}\left[f_L(\mathbf{Q}) + f_{EL}(\mathbf{Q}, \nabla\mathbf{Q}) + f_{EF}(\mathbf{Q}, E_f)\right] + \oint d^2\mathbf{x} f_S(\mathbf{Q}) \quad (4)$$

The Landau free energy density f_L is a phenomenological approximation obtained as a truncated expansion with respect to the invariants of Q:

$$f_L[\mathbf{Q}] = \frac{A}{2}\left(1-\frac{U}{3}\right)\mathrm{tr}\left(\mathbf{Q}^2\right) - \frac{AU}{3}\mathrm{tr}\left(\mathbf{Q}^3\right) + \frac{AU}{4}\mathrm{tr}\left(\mathbf{Q}^2\right)^2, \quad (5)$$

where parameter *A* sets an energy density scale for the model. A dimensionless parameter *U* determines the IN transition. [3–5] For Eqn. (5), we adopt Doi's notation and consider a unique value for the energy scale *A*. [6, 7]

Assuming one elastic constant approximation, the elastic contribution is given in terms of gradients of the alignment tensor according to: [8–10]

$$f_{EL} = \frac{1}{2}L_1\frac{\partial Q_{ij}}{\partial x_k}\frac{\partial Q_{ij}}{\partial x_k} + \frac{1}{2}L_2\frac{\partial Q_{jk}}{\partial x_k}\frac{\partial Q_{jl}}{\partial x_l} + \frac{1}{2}L_3 Q_{ij}\frac{\partial Q_{kl}}{\partial x_i}\frac{\partial Q_{kl}}{\partial x_j} \quad (6)$$

where L_1, L_2 and L_3 are the elastic constants. For a uniaxial system, the elastic constants in Eqn. (6) are related to the first order Frank-Oseen [10–13] elastic constants through

$$L_1 = \frac{1}{6S^2}\left(k_{33} - k_{11} + 3k_{22}\right) \quad (7)$$

$$L_2 = \frac{1}{S^2}\left(k_{11} - k_{22}\right) \quad (8)$$

$$L_3 = \frac{1}{2S^3}\left(k_{33} - k_{11}\right) \quad (9)$$

where *S* is the scalar order parameter and k_{11}, k_{22} and k_{33} are non-vanishing elastic moduli corresponding to the independent splay, twist and bend. [1]

The surface contributions to the free energy describe the interaction of the liquid crystal with boundaries or interfaces. For homeotropic anchoring, a harmonic Rapini-Papoular [14–18] term is used:

$$f_{S,\mathrm{R}}[\mathbf{Q}] = \frac{1}{2}W\left(\mathbf{Q}-\mathbf{Q}_\perp\right)^2 \quad (10)$$

where *W* represents the strength of the anchoring, $\mathbf{Q}_\perp = S[\boldsymbol{\nu}\boldsymbol{\nu} - {}^1\!/_3\boldsymbol{\delta}]$ is the perpendicular tensor preferred at the surface, and $\boldsymbol{\nu}(x)$ is the normal unit vector at any point *x* on the surface. For degenerate planar anchoring, a 4th order Fournier-Galatola energy density is adopted: [19]

$$f_{S,\mathrm{F}}[\mathbf{Q}] = \frac{1}{2}W\left(\overline{\mathbf{Q}}-\overline{\mathbf{Q}}_\perp\right)^2 + \frac{1}{4}W\left(\overline{\mathbf{Q}}:\overline{\mathbf{Q}} - S^2\right)^2 \quad (10)$$

where $\overline{\mathbf{Q}} = \mathbf{Q} + S\boldsymbol{\delta}/3$, $\overline{\mathbf{Q}}_{\perp} = \mathbf{p} \cdot \overline{\mathbf{Q}} \cdot \mathbf{p}$ is the tensor's projection on the surface, and $\mathbf{p} = \boldsymbol{\delta} - \boldsymbol{\nu}\boldsymbol{\nu}$.

The physical properties of the LC serve to define two characteristic length scales: the nematic coherence length ξ_N which is related to the spatial scale over which the local fluctuations are correlated; [20] and the surface extrapolation length ξ_S. These are given by:

$$\xi_N = \sqrt{L_1/A} \quad , \quad \xi_S = L_1/W. \tag{12}$$

The latter scale is also known as the Kleman-de Gennes extrapolation distance, and it defines the relative strength of the nematic elasticity on the bulk with respect to the surface anchoring strength. [21, 22] Parameters in the simulations are non-dimensionalized in terms of the nematic coherence length ξ_N and material parameter A. The free energy functional of the system can thus be expressed in a dimensionless form as

$$\hat{F}(\mathbf{Q}) = \frac{F(\mathbf{Q})}{A\xi_N^3} \tag{13}$$

For simplicity, all functions and variables are assumed to be dimensionless throughout the remainder of this manuscript.

The free energy term associated to the electric field contribution is given by the equation:

$$f_{ef} = -\epsilon_a E_\alpha Q_{\alpha\beta} E_\beta \tag{14}$$

where E_α is the external electric field applied on the system and ϵ_a is the dielectric anisotropy.

NUMERICAL RELAXATION

The idea behind the MC relaxation is to generate a Markov chain of states and to use a Metropolis scheme to relax the free energy, during a fluctuating temperature annealing. In particular, appropriate random updates to the alignment tensor field are

generated, and they are accepted or rejected ensuring that detailed balance is maintained. A Markov chain of configurations is constructed by proposing transitions between an old configuration "*o*" and a new one "*n*" with probability $P_{acc}(o \rightarrow n)$, accepting such transitions with a probability:

$$P_{acc}(o \rightarrow n) = min\,[1, -\beta \Delta F] \quad (15)$$

where $\Delta F = F(\mathbf{Q}(n)) - F(\mathbf{Q}(o))$ is the energy difference between the new and old configurations and $\beta^{-1} = k_B \hat{T}$ (k_B is Boltzmann constant). An annealing process is used to minimize the free energy functionals, according to the fluctuating temperature $\hat{T}$ [23, 24]. The simulation starts with a high non-dimensional fluctuating temperature $T = A\xi_N^3 / \beta$, used in the Metropolis criterion. The majority of MC moves are accepted as the fluctuations dominate, resulting in an isotropic state. The temperature is then progressively lowered until the LC system achieves an equilibrium state. We found the most efficient annealing to follow an exponential temperature decrease. Typically, $10 < \beta < 10^{12}$ over the total MC minimization.

To obtain the Markov chain, the Hamiltonian $F = F(\xi_N, \xi_S, \mathbf{a}, \nabla\mathbf{a})$ (Eq. (2)), is discretized over a mesh and it is integrated numerically. A point $\boldsymbol{x}$ is selected randomly, in the bulk or surface, and an MC move is attempted by a random displacement on $\boldsymbol{a}(\boldsymbol{x})$:

$$a_{\mu,n}(\mathbf{x}) = a_{\mu,o}(\mathbf{x}) + \bar{\delta_\mu}(\xi_1 - 0.5), \quad (16)$$

where component μ is selected randomly from 1 to 5, ξ_1 is a random number from a uniform distribution on [0, 1] and $\bar{\delta}_\mu$ is the maximum allowed perturbation for a_μ.

For this minimization method, we have expressed Q in terms of an orthonormal tensor basis as discussed by Hess and co-workers [25]and more recently by Bhattacharjee et al.:

26, 27

$$\mathbf{Q}(\mathbf{x},t) = \sum_{\nu}^{5} a_{\nu}(\mathbf{x},t)\mathbf{T}^{\nu}, \qquad (17)$$

where the orthonormal basis is defined by five tensors:

$$\begin{aligned}
\mathbf{T}^1 &= \sqrt{3/2}\,[\hat{\mathbf{z}}\hat{\mathbf{z}}]^{\mathrm{ST}} = \sqrt{3/2}\,(\delta_{3i}\delta_{3j} - \delta_{ij}/3)\,,\\
\mathbf{T}^2 &= \sqrt{2}\,[\hat{\mathbf{x}}\hat{\mathbf{y}}]^{\mathrm{ST}} = \sqrt{2}\,(\delta_{1i}\delta_{2j} + \delta_{2i}\delta_{1j})\,/2,\\
\mathbf{T}^3 &= \sqrt{2}\,[\hat{\mathbf{x}}\hat{\mathbf{z}}]^{\mathrm{ST}} = \sqrt{2}\,(\delta_{1i}\delta_{3j} + \delta_{3i}\delta_{1j})\,/2,\\
\mathbf{T}^4 &= \sqrt{1/2}\,(\hat{\mathbf{x}}\hat{\mathbf{x}} - \hat{\mathbf{y}}\hat{\mathbf{y}}) = \sqrt{1/2}\,(\delta_{1i}\delta_{1j} - \delta_{2i}\delta_{2j})\,,\\
\mathbf{T}^5 &= \sqrt{2}\,[\hat{\mathbf{y}}\hat{\mathbf{z}}]^{\mathrm{ST}} = \sqrt{2}\,(\delta_{2i}\delta_{3j} + \delta_{3i}\delta_{2j})\,/2. \qquad (18)
\end{aligned}$$

where ***x***, ***y*** and ***z*** are the canonic $\mathfrak{R}^3$ basis, $[\boldsymbol{A}]^{ST}$ is the symmetric-traceless projection operation and δ_{ij} is the Kronecker delta. Because the $\{\boldsymbol{T}^m\}$ basis is orthonormal

$$\mathrm{tr}(\mathbf{T}^m\mathbf{T}^n) = T^m_{ij}T^n_{ij} = \delta_{mn}, \qquad (19)$$

ensures that the five scalar components a_ν of the alignment tensor are simple projections:

$$a_{\nu} = \mathrm{tr}\left(\mathbf{Q}\mathbf{T}^{\nu}\right). \qquad (20)$$

They provide a unique and independent way to define a specific configuration of the alignment tensor field. Note that because the alignment tensor is expressed in the orthonormal tensor basis, a MC move defined by Eq. (16) implies a uniform sampling over the tensor's proper values *S*, η, ***n*** and ***n′***. In addition, for every MC move, the tensor at ***x***, the amount of perturbation and the orthonormal basis are selected randomly; a single basis μ is modified in each MC step, ensuring an efficient MC. The maximum displacement $\bar{\delta}_{\mu}$ is modified dynamically during the minimization to enforce that each basis has a 30% acceptance.

Finite Element Approach. The free energy functional is minimized to identify the equilibrium phases through an annealing MC relaxation technique. [23,24] The free energy integration is carried out by a Legendre-Gauss quadrate on a finite element discretization scheme, with six-noded isoparametric tetrahedral elements that describe all variables and fields. The quadrature integration [28] on the elements results in an O(1) MC algorithm. Cubit®, under the Argonne National Laboratory's license, [29] was used to generate the tetrahedral meshes and LibMesh [30] libraries served to optimize and parameterize the original Cubit meshes. The simulated systems were composed of 4×10^6 elements. Typical relaxations required 4×10^5 average MC moves per element, where 30% acceptance was enforced with the MC step and an exponential temperature annealing was imposed to avoid local entrapment.

Theoretical crossed polarizer. Crossed polarizer images were obtained through simulations based on the matrix Jones formalism that allows us to model the changes in polarization and phase shift when the light passes through the channel system. Let the wave vector of a ray ***k*** be parallel to the z-axis, passing through the positions (x_0, y_0, z). The intensity is given by $I(z) = \|\|e_A T(z) e_p\|\|$, where e_A is the orientation of the analyzer and e_p is the incident polarization. $T(z)$ corresponds to the transformation matrix which accounts for the rotation of the polarization vector and for appropriate phase shifts. We assume the path of the ray is discretized in N segments of length equal to the mesh resolution, ξ_N, then the transformation matrix is given by [31]

$$\mathbf{T(z)} = \mathbf{R_{N+1} S_N R_N \cdots S_2 R_2 S_1 R_1}, \quad (23)$$

where the rotation matrix, $\boldsymbol{R_i}$, is

$$\mathbf{R_i} = \begin{pmatrix} \cos(\alpha_i - \alpha_{i-1}) & -\sin(\alpha_i - \alpha_{i-1}) \\ \sin(\alpha_i - \alpha_{i-1}) & \cos(\alpha_i - \alpha_{i-1}) \end{pmatrix} \quad (24)$$

where α is the angle between the projection of local nematic director on the *xy* plane and e_p. The phase shift matrix, ***S***, reads,

$$\mathbf{S_i} = \begin{pmatrix} \exp(i2\pi n_0 \xi_N/\lambda_0) & 0 \\ 0 & \exp(i2\pi n_e(\gamma_i)\xi_N/\lambda_0) \end{pmatrix}, \quad (25)$$

where γ is the angle between the local nematic director and the wave vector; n_o and $n_e(\gamma)$ represent the ordinary and extraordinary refraction indexes. n_o is 1.5 while n_e is given by

$$n_e(\gamma_i) = \frac{n_0 n_e}{\sqrt{n_0^2 \sin^2(\gamma_i) + n_e^2 \cos^2(\gamma_i)}} \quad (26)$$

with n_e = 1.7. [31]

References:

(1) Lubensky, T. C. Molecular Description of Nematic Liquid Crystals. *Phys. Rev. A-Gen. Phys.* **1970**, 2, 2497-2514.

(2) Saupe, A. Elastic and Flow Properties of Biaxial Nematics. *J. Chem. Phys.* **1981**, 75, 5118-5124.

(3) Guzmán, O.; Abbott, N. L.; de Pablo J. J. Defect Structures and Three-Body Potential of the Mean Force for Nanoparticles in a Nematic Host. *J. Poly. Sci. B* **2005**, 43, 1033-1040.

(4) Guzmán, O.; Abbott, N. L.; de Pablo J. J. Quenched Disorder in a Liquid-Crystal Biosensor: Adsorbed Nanoparticles at Confining Walls. *J. Chem. Phys.* **2005**, 122, 184711.

(5) Grollau, S.; Guzmán, O.; Abbott, N. L.; de Pablo J. J. Slow Dynamics of Thin Nematic Films in the Presence of Adsorbed Nanoparticles. *J. Chem. Phys.* **2005**, 122, 024703.

(6) Beris, A. N.; Edwards, B. J. Thermodynamics of Flowing Systems. *Oxford University Press*: Oxford **1994**.

(7) de Gennes, P.; Prost, J. The Physics of Liquid Crystals. *2nd edn Oxford Science Publications*: Oxford **1993**.

(8) Nehring, J.; Saupe, A. Calculation of Elastic-Constants of Nematic Liquid Crystals. *J. Chem. Phys*. **1972**, 56, 5527-5528.

(9) Nehring, J.; Saupe, A. Elastic Theory of Uniaxial Liquid Crystals. *J. Chem. Phys*. **1971**, 54, 337-343.

(10) Mori, H.; Gartland, E. C.; Kelly, J. R.; Bos, P. J. Multidimensional Director Modeling Using the *Q* Tensor Representation in a Liquid Crystal Cell and Its Application to the *pi* Cell with Patterned Electrodes. *Jpn. J. Appl. Phys.* **1999**, 38, 135-146.

(11) Oseen, C. The Theory of Liquid Crystals. *Trans. Faraday Soc.* **1933**, 29, 883-898.

(12) Mr. Bernal; Dr. Lawrence; Prof. Oseen; Zocher, H.; Dr. Kast; Prof. Ornstein; Mr. Feachem; Adam, N. K.; Prof. Desch; Prof. Lowry; Mr. Rawlins; Prof. Herrmann; Prof. Foëx; Dr. Malkin; Prof. Porter; Prof. Stewart; Stewart, G. W.; Taylor, A. M.; Prof. Ostwald; Mr. Carpenter, *et al.* Liquid Crystals and Anisotropic Melts. A General Discussion. *Trans. Faraday Soc*. **1933**, 29, 1060-1085.

(13) Frank, F. On the Theory of Liquid Crystals. *Discuss. Faraday Soc.* **1958**, 25, 19-28.

(14) Papoular, M.; Rapini, A. Surface Waves in Nematic Liquid Crystals. *Solid State Commun.* **1969**, 7, 1639-1641.

(15) Nobili, M.; Durand, G. Disorientation-Induced Disordering at a Nematic Liquid Crystal Solid Interface. *Phys. Rev. A* **1992**, 46, R6174-R6177.

(16) Ravnik, M.; Alexander, G. P.; Yeomans, J. M.; Zumer, S. Mesoscopic Modelling of Colloids in Chiral Nematics. *Faraday Discuss*. **2010**, 144, 159-169.

(17) Skarabot, M.; Ravnik, M.; Zumer, S.; Tkalec, S.; Poberaj, I.; Babic, D.; Osterman, N.; Musevic, I. Two-Dimensional Dipolar Nematic Colloidal Crystals. *Phys. Rev. E* **2007**, 76, 051406.

(18) Hung, F. R. Quadrupolar Particles in a Nematic Liquid Crystal: Effects of Particle Size and Shape. *Phys. Rev. E* **2009**, 79, 021705.

(19) Fournier, J.; Galatola, P. Modeling Planar Degenerate Wetting and Anchoring in Nematic Liquid Crystals. *Europhys. Lett.* **2005**, 72, 403-409.

(20) Vertogen, G.; d. Jeu, W. H. Thermotropic Liquid Crystals, Fundamentals. *Springer-Verlag Berlin*: New York **1987**.

(21) Kleman. M.; Williams, C. Anchoring Energies and Nucleation of Surface Disclination Lines in Nematic. *Philos. Mag.* **1973**, 28, 725-732.

(22) Ravnik, M.; Zumer, S. Landau-de Gennes Modelling of Nematic Liquid Crystal Colloids. *Liq. Cryst.* **2009**, 36, 1201-1214.

(23) Armas-Perez, J. C.; Hernandez-Ortiz, J. P.; de Pablo, J. J. Liquid Crystal Free Energy Relaxation by a Theoretically Informed Monte Carlo Method Using a Finite Element Quadrature Qpproach. *J. Chem. Phys.* **2015**, 143, 243157.

(24) Armas-Perez, J. C.; Londono-Hurtado, A.; Guzman, O.; Hernandez-Ortiz, J. P.; de Pablo, J.J. Theoretically Informed Monte Carlo Simulation of Liquid Crystals by Sampling of Alignment-Tensor Fields. *J. Chem. Phys.* **2015**, 143, 044107.

(25) Kaiser, P.; Wiese, W.; Hess, S. Stability and Instability of an Uniaxial Alignment Against Biaxial Distortions in the Isotropic and Nematic Phases of Liquid Crystals. *J. Non-Equilib. Thermodyn.* **1992**, 17, 153-169.

(26) Bhattacharjee, A. K.; Menon, G. I.; Adhikari, R. Numerical Method of Lines for the Relaxational Dynamics of Nematic Liquid Crystals. *Phys. Rev. E* **2008**, 78, 026707.

(27) Bhattacharjee, A. K.; Menon, G. I.; Adhikari, R. Fluctuating Dynamics of Nematic Liquid Crystals Using the Stochastic Method of Lines. *J. Chem. Phys.* **2010,** 133, 044112.

(28) Osswald, T. A.; Hern´andez-Ortiz, J. P. Polymer Processing: Modeling and Simulation (Carl Hanser-Verlag, Munich, **2006**).

(29) CUBIT, Version 14.1, Sandia National Laboratories, **2014**.

(30) Kirk, B. S.; Peterson, J. W.; Stogner, R. H.; Carey, G. F. libMesh: A C++ Library for Parallel Adaptive Mesh Refinement/Coarsening Simulations. *Eng. Computers* **2006**, 22, 237-254.

(31) Ondris-Crawford, R.; Boyko, E. P.; Wagner, B. G.; Erdmann, J. H.; Zumer, S.; Doane, J. W. Microscope Textures of Nematic Droplets in Polymer Dispersed Liquid Crystals. *J. Appl. Phys.* **1991**, 69, 6380-6386.